


A Transformer-Based Adaptive Semantic Aggregation Method for UAV Visual Geo-Localization

Shishen Li, Cuiwei Liu , Huaijun Qiu, and Zhaokui Li

School of Computer Science, Shenyang Aerospace University, Shenyang, China
liucuiwei@sau.edu.cn

Abstract. This paper addresses the task of Unmanned Aerial Vehicles (UAV) visual geo-localization, which aims to match images of the same geographic target taken by different platforms, i.e., UAVs and satellites. In general, the key to achieving accurate UAV-satellite image matching lies in extracting visual features that are robust against viewpoint changes, scale variations, and rotations. Current works have shown that part matching is crucial for UAV visual geo-localization since part-level representations can capture image details and help to understand the semantic information of scenes. However, the importance of preserving semantic characteristics in part-level representations is not well discussed. In this paper, we introduce a transformer-based adaptive semantic aggregation method that regards parts as the most representative semantics in an image. Correlations of image patches to different parts are learned in terms of the transformer’s feature map. Then our method decomposes part-level features into an adaptive sum of all patch features. By doing this, the learned parts are encouraged to focus on patches with typical semantics. Extensive experiments on the University-1652 dataset have shown the superiority of our method over the current works.

Keywords: UAV visual geo-localization · transformer · part matching.

1 Introduction

Unmanned Aerial Vehicle (UAV) visual geo-localization refers to cross-view image retrieval between UAV-view images and geo-tagged satellite-view images. Recently, this technology has been applied in many fields, such as precision agriculture [1], rescue system [2], and environmental monitoring [3]. Using a UAV-view image as the query, the retrieval system searches for the most relevant

This work was supported in part by the National Natural Science Foundation of China (NSFC) under Grant No.62171295, and in part by the Liaoning Provincial Natural Science Foundation of China under Grant No.2021-MS-266, and in part by the Applied Basic Research Project of Liaoning Province under Grant 2023JH2/101300204, and in part by the Shenyang Science and Technology Innovation Program for Young and Middle-aged Scientists under Grant No.RC210427, and in part by the High Level Talent Research Start-up Fund of Shenyang Aerospace University under Grant No.23YB03.

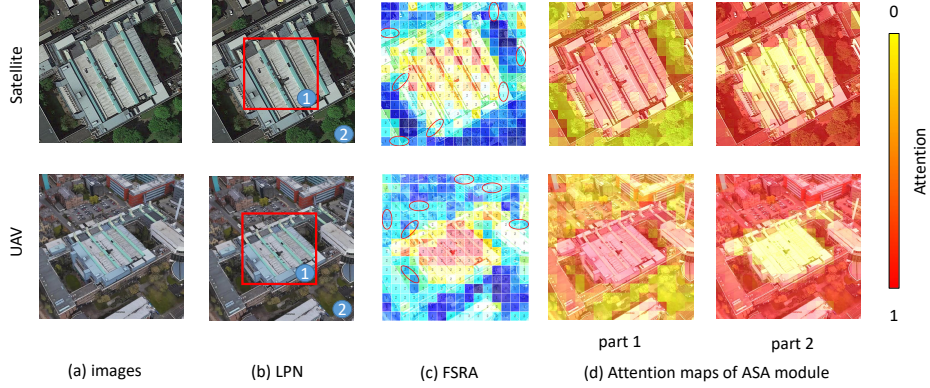


Fig. 1. An UAV-satellite image pair is shown in column(a). The square-ring partition strategy of LPN [5] is depicted in column(b). Column(c) illustrates the heat map and the part partition of image patches generated by FSRA [6]. Red ellipses mark patches that are similar in features but divided into different parts. Attention maps corresponding to two parts produced by the proposed ASA module are given in column(d).

satellite-view candidate to determine the geographic location of the UAV-view target. On the other hand, if a satellite-view image is used as the query, the corresponding UAV-view images can be retrieved from the UAV flight records, enabling UAV navigation. Compared to traditional geo-localization methods that rely on GPS or radar, UAV visual geo-localization does not require the UAV to receive external radio information or emit detection signals, making it possible to achieve UAV positioning and navigation in radio silence.

The key to UAV visual geo-localization is to extract discriminative features. Specifically, satellites acquire fixed-scale images from a vertical view, while UAVs take images from various distances and orientations at an oblique view, resulting in large visual and scale variations in UAV-satellite image pairs. Moreover, images of different locations share some local patterns, such as vegetation and similarly styled buildings, which also pose challenges to cross-view image retrieval. These issues make hand-crafted descriptors (e.g., SIFT [4]) perform poorly.

Early UAV visual geo-localization methods employ two-branch CNN models [7, 8] to achieve cross-view matching between UAV-view and satellite-view images. Benefiting from the availability of multiple UAV-view images of the same location, the models are optimized in a location classification framework to learn view-invariant yet location-dependent features. By doing this, two-branch CNN models are desired to generate similar features for satellite-view and UAV-view images taken at a new location that is unseen during training. However, the learned features focus on the entire image, while neglecting fine-grained details that are crucial for distinguishing images of different locations. Upon two-branch CNN models, Local Pattern Network (LPN) [5] divides the feature map into several regions with square-rings to extract part-level representations as shown in Fig. 1 (b). Then part matching is performed to roughly align the geographic targets as well as their surroundings. Another iconic work is a two-branch

transformer-based model called FSRA (Feature Segmentation and Region Alignment) [6], which clusters image patches into semantic parts according to the heat distribution of feature maps as shown in Fig. 1 (c). Each part is desired to indicate certain semantics such as target or surroundings. Compared to LPN that adopts fixed-scale spatial partition, FSRA is more flexible in extracting parts and thus more robust against image shift and scale variations. However, FSRA employs a hard partition strategy where an image patch belongs to only one part and the part-level representations are calculated as mean of image patches. We argue that there are two issues pertaining to such strategy. First, image patches similar in features may be divided into different parts as shown in Fig. 1 (c). Secondly, such strategy cannot extract the most representative semantics since it neglects the associations between image patches and parts.

To cope with these limitations, this paper proposes an Adaptive Semantic Aggregation (ASA) module. Unlike the hard partition strategy utilized in FSRA [6], the ASA module employs a soft partition strategy that considers correlations between parts and all image patches to generate global-aware part-level representations. Specifically, each part is regarded as one semantic and has a distribution of attention over all image patches as shown in Fig. 1 (d). First, the most representative patch is selected as anchor of a part. Attentions of image patches are allocated by calculating similarities between patches and the anchor. A high attention expresses strong correlation of an image patch to the semantic part, while a low attention indicates weak correlation. Then all patch-level features are adaptively aggregated into global-aware part-level representations according to the learned attentions. Finally, the ASA module is integrated into the two-branch transformer-based framework [6] and explicitly enables the learned parts focus on distinctive patches, such as gray roof and circular road.

The remainder of this paper is organized as follows. Section 2 briefly describes the current work related to cross-view geo-localization. Section 3 introduces the overall framework of our method and describes the proposed ASA module in detail. Section 4 presents and analyzes the experimental results on the University-1652 dataset. Section 5 summarizes this paper.

2 Related Work

In 2020, Zheng et al. [7] formulated the UAV visual geo-localization problem as bidirectional cross-view image retrieval between UAV-view and satellite-view images. They employed a two-branch CNN model to extract global features from different domains and released the University-1652 dataset for model evaluation. Upon this work, Ding et al. [8] simplified the cross-view image retrieval task as a location classification problem during training, aiming to learn a common location-dependent feature space that is well scalable for unseen images. They noticed the imbalance of UAV-view and satellite-view images, and performed data augmentation to expand training satellite-view images. Based on the above location classification framework, recent works [5, 6, 9–12] have made various attempts to improve the discriminative power of the learned feature space.

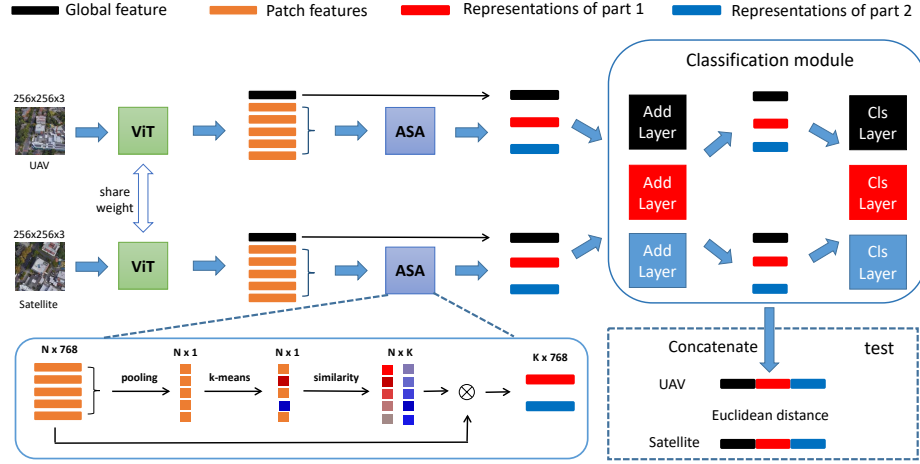


Fig. 2. Overall framework of our method.

One typical solution is LPN [5] which achieves fine-grained part matching between UAV-view and satellite-view images. LPN applies a square-ring partition strategy to separate global feature maps into multiple parts according to their spatial position. Then rotation-invariant part-level features are obtained by performing average pooling over points within each part. Tian et al. [9] produces synthesized UAV-view images by a generative model to reduce the gap between two views. Then they employed LPN [5] to achieve cross-view image retrieval. Zhuang et al. [10] improved LPN [5] by incorporating global features and adding KL loss to further close the distance between paired UAV-view and satellite-view images. Lin et al. [11] introduced a Unit Subtraction Attention Module (USAM) that forces the geo-localization model (e.g., LPN [5]) to focus on salient regions by detecting representative key points.

Considering that the square-ring partition strategy is not robust to scale variations, Dai et al. [6] aimed to extract semantic parts composed of patches scattered throughout the image. Small patches are ranked according to the feature heat map and uniformly divided into multiple parts, regardless of their spatial position. Then a part is represented by the average feature of patches within it. Zhuang et al. [12] improved this part partition strategy by searching for the optimal split based on the gradient between adjacent positions in the ranking results. However, the above methods [6, 12] aggregate image patches equally, thus weakening the semantic characteristics of the learned parts. In this paper, we propose an Adaptive Semantic Aggregation module that regards parts as the most representative semantics in images and obtains part-level features by aggregating all patch features based on their correlations to parts.

3 Method

Fig. 2 depicts the overall framework of our method. Inspired by siamese networks [13, 14], two branches are designed to handle images captured by UAVs

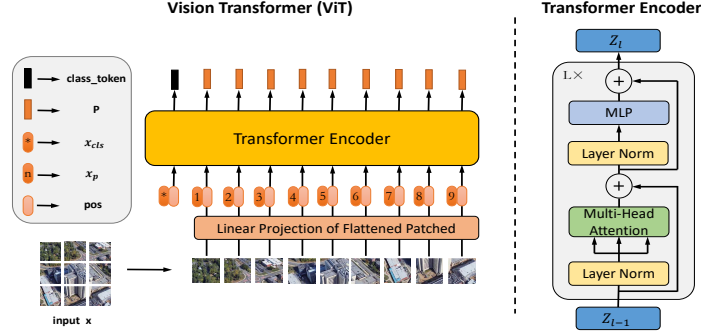


Fig. 3. Architecture of Vision Transformer (ViT).

and satellites respectively. Following FSRA [6], we adopt ViT (Vision Transformer) [15] as the backbone to extract features from both UAV-view images and satellite-view images. Backbones of the UAV branch and the satellite branch share weights to learn a mapping function that is able to project images from both views to one common embedding space. ViT produces global features of the entire image as well as local features of image patches that are fed into the proposed ASA module to generate multiple part-level representations. Finally, global features and part-level representations are sent to the classification module, which regards geographic locations of training images as semantic categories. The classification module contains additive layers for representation transformation and classification layers for geo-location prediction.

In the test stage, our goal is to achieve cross-view retrieval between UAV-view and satellite-view images captured at new geographic locations. That is to say, the classifier cannot infer locations of query or gallery images during test, since the test data have their own location label space disjoint with the training data. Therefore, we concatenate the transformed representations before classification layers in the classifier module as the final descriptor of a test image. In order to measure the correlation between a query image from one view and gallery images from another view, we calculate the euclidean distance between them. Finally, we sort gallery images in terms of their distance to the query image and return the most similar one to achieve cross-view image retrieval.

3.1 Transformer-based backbone

Architecture of our backbone is illustrated in Fig. 3. Given an input image $x \in R^{H \times W \times C}$, it is first divided into fixed-size patches using pre-defined parameters. Then patches are linearly transformed to obtain embedding vectors $x_p \in R^{N \times D}$, where N and D refer to the number of patches and the embedding dimension, respectively. Additionally, a learnable vector $x_{cls} \in R^{1 \times D}$ forwards along with x_p . All these embedding vectors are integrated with position embeddings $pos \in R^{(N+1) \times D}$ to obtain input vectors Z_0 of the Transformer Encoder. This procedure is formulated by

$$Z_0 = [x_{cls}; x_p] + pos. \quad (1)$$

To accommodate the varying resolution of input images, we employ learnable position embeddings instead of utilizing parameters pre-trained on ImageNet [16].

As shown in Fig. 3, the Transformer Encoder consists of alternating Multiple Head Self-Attention layers and Layer Norm (LN) operations, where residual connections are applied. Multi-Layer Perceptron (MLP) is a two-layer non-linearity block, each layer of which ends with a GELU activation function. The process of Transformer Encoder is formulated by

$$Z'_l = MHSA(LN(Z_{l-1})) + Z_{l-1}, \quad (2)$$

$$Z_l = MLP(LN(Z'_l)) + Z'_l, \quad (3)$$

where Z'_l and Z_l denote output vectors of the l^{th} attention layer and the l^{th} MLP layer, respectively. Finally, the output vector Z_L consists of a global feature *class.token* $\in R^{1 \times D}$ generated upon x_{cls} and patch-level features $\{P_i \in R^{1 \times D}\}_{i=1:N}$ generated from x_p .

3.2 Adaptive semantic aggregation module

Previous works have shown the effectiveness of part matching between UAV-view and satellite-view images in the UAV-view geo-localization task. In this paper, we propose a soft partition strategy to adaptively aggregate image patches into part-level representations. Different from hard partition strategies [5,6], the proposed soft partition strategy regards a part as semantic aggregation of image patches according to correlations between them. Details of the ASA module are illustrated in Fig. 2.

An input image x is first fed into ViT to extract global features as well as patch-level features $\{P_i \in R^{1 \times D}\}_{i=1:N}$. Assuming equal importance of feature dimensions, we apply average pooling on features of each patch to obtain 1-dimensional representations, denoted as $\{Q_i \in R^{1 \times 1}\}_{i=1:N}$.

$$Q_i = \frac{1}{D} \sum_{d=1}^D P_i^d, \quad (4)$$

where i and d represent the indices of patch and feature dimension, respectively. Patches with similar semantic information exhibit similar representations in $\{Q_i\}_{i=1:N}$, as demonstrated in FSRA [6] (see Fig. 1 (c)). Accordingly, we perform k-means algorithm upon $\{Q_i\}_{i=1:N}$ to extract representative semantics.

Specifically, the 1-dimensional representations are first sorted in descending order to obtain a sequence S , each item in which indicates a patch index. We introduce a hyper-parameter K , which denotes the number of semantic categories in the image. Center of the k^{th} category is initialized as 1-dimensional representations of a patch S_{IC_k} , and the index IC_k is denoted by

$$IC_k = \frac{(2k-1)N}{2K}. \quad k = 1, 2, \dots, K \quad (5)$$

The k-means algorithm updates semantic categories iteratively and outputs the final category centers. Center of the k^{th} category corresponds to a patch P_{C_k} , which is regarded as the anchor of a part. Then we utilize the original patch features produced by ViT to calculate Euclidean distance dis_k^i between anchor of a part and all image patches. This procedure is formulated by

$$dis_k^i = ||P_i - P_{C_k}||_2. \quad (6)$$

Given the negative correlation between distance and similarity, we employ the cosine function to obtain the attention matrix by

$$A_k^i = \alpha \cdot \cos\left(\frac{dis_k^i - dis_k^{min}}{dis_k^{max} - dis_k^{min}} \cdot \frac{\pi}{2}\right) + \beta, \quad (7)$$

where α and β are factors for enhancing the robustness of the weight matrix and are respectively set to 1 and 0 in our specific experiments. Finally, we aggregate patch features $\{P_i\}_{i=1:N}$ into global-aware part-level features $\{\rho_k\}_{k=1:K}$ according to the customized attention matrix A .

$$\rho_k = \frac{\sum_{i=1}^N P_i \cdot A_k^i}{\sum_{i=1}^N A_k^i}. \quad (8)$$

It should be noted that 1-dimensional semantic representations $\{Q_i\}_{i=1:N}$ are utilized to find anchors of parts at low clustering cost, while original D-dimensional features $\{P_i\}_{i=1:N}$ are employed for feature aggregation. In fact, clustering results of the k-means algorithm can also be used to achieve a hard partition strategy, which is compared to the proposed soft partition strategy on the University-1652 dataset in Section 4.

3.3 Classification module

The classification module takes global features as well as part-level representations as input, aiming at classifying them into different geographic locations. As shown in Fig. 4, the classification module consists of additive layers and classification layers. The former achieve transformation of the input while the latter produce prediction vectors of geographic locations. Separate layers are constructed for global features and representations of each part, considering that they indicate different semantic characteristics. Take representations of the k^{th} part as an example, operations of the classification module can be formulated as

$$f_k = F_{add}^k(\rho_k), \quad (9)$$

$$z_k = F_{cls}^k(f_k), \quad (10)$$

where F_{add}^k and F_{cls}^k represents the additive layer and the classification layer for the k^{th} part, respectively. f_k denotes output features of the additive layer and z_k indicates predicted logits for all geographic locations.

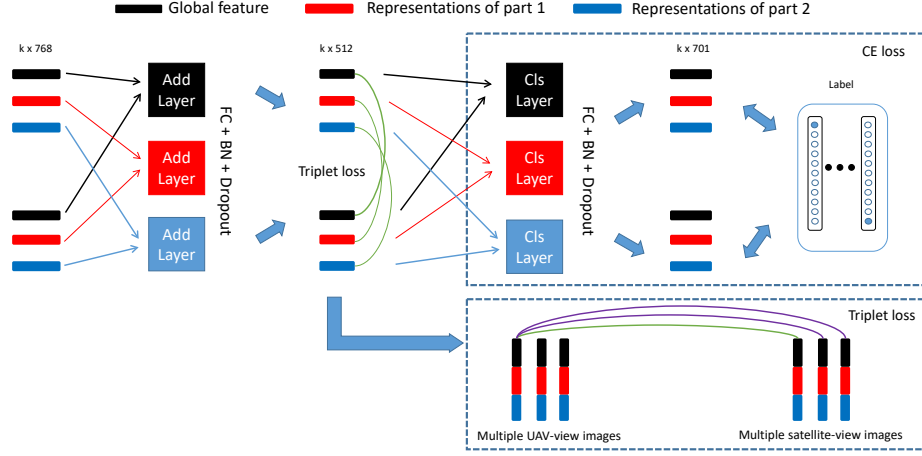


Fig. 4. Architecture of the classification module. In training, global and part-level features are fed into additive layers followed by classification layers. Suppose that the training data come from 701 locations, so a classification layer predicts a 701-dimensional vector. The model is optimized by CE loss and Triplet loss. Green and purple lines point at positive and negative samples for calculating the Triplet loss, respectively.

Following [6], the model is optimized by both CE loss L_{CE} and Triplet Loss $L_{Triplet}$. The total objective is defined as

$$L_{total} = L_{CE} + L_{Triplet}, \quad (11)$$

where L_{CE} is the cross entropy between the predicted logits and the ground-truth geo-tags, formulated by

$$L_{CE} = -\frac{1}{K} \sum_{i=1}^K \log \frac{\exp(z_k(y))}{\sum_{c=1}^C \exp(z_k(c))}, \quad (12)$$

where C indicates the number of geographic locations in the training data and $z_k(y)$ is the logit score of the ground-truth geo-tag y . The Triplet Loss is performed on the output features of additive layers to pull paired UAV-view and satellite-view images together, while pushing away mismatched image pairs. The Triplet Loss is formulated by

$$L_{TripletLoss} = \frac{1}{K} \sum_{i=1}^K \max(d(f_k, p) - d(f_k, n) + M; 0), \quad (13)$$

Where M is a hyper-parameter and empirically set to 0.3. $d(\cdot)$ represents the distance function. p and n indicate positive sample and negative samples, respectively. As depicted in Fig. 4, both the positive (green line) and negative samples (purple lines) come from another view. For example, if we take part-level feature f_k of a UAV-view image as the anchor, then f_k is compared to the corresponding part features of the true-matched and mismatched satellite-view images.

4 Experiments

4.1 Dataset

University-1652 dataset [7] contains images of 1652 buildings from 72 universities in three different camera views, i.e. UAV view, satellite view, and ground view. This dataset is employed to evaluate the proposed method on the UAV visual geo-localization task, so only UAV-view and satellite-view images are utilized to achieve bidirectional cross-view image retrieval. For each building, one image was obtained by satellites and 54 images were captured by UAVs at different heights and perspectives. Thus, there exist large variations in image scale and viewpoints, which poses great challenges to the UAV visual geo-localization task.

The dataset is split into a training set including 38,555 images of 701 buildings from 33 universities and a test set containing 52,306 images of 951 buildings from the reminder 39 universities. During training, we number 701 buildings into 701 different categories of the classification module and learn an embedding space for UAV-view and satellite-view images. In the UAV-to-satellite image retrieval task, the query set consists of 37,855 UAV-view images of 701 buildings and the gallery includes 701 true-matched satellite-view images and 250 distractors. In the satellite-to-UAV image retrieval task, 701 satellite-view images constitute the query set and there are 51,355 gallery images, including 37,855 true-matched UAV-view images and 13,500 distractors from the rest 250 buildings.

4.2 Evaluation protocol

Following the previous works [5, 7–10], we employ two types of evaluation metrics, namely Recall@K and average precision (AP). Recall@K and AP are widely applied in image retrieval tasks. Recall@K refers to the ratio of query images with at least one true-matched image appearing in the top-K ranking list. AP computes the area under the Precision-Recall curve and considers all true-matched images in the gallery. Recall@K focuses on the position of the first true-matched image in the matching results and thus is suitable for evaluation on the UAV-to-satellite image retrieval task where the gallery only contains one true-matched satellite-view image for each UAV-view query. In the satellite-to-UAV image retrieval task, there are multiple true-matched UAV-view images for one satellite-view query and AP is able to comprehensively measure the matching results. In this paper, we report the mean Recall@K and mean AP of all queries.

4.3 Implementation details

All the input images are resized to 256×256 and the number of parts (K) is set to 2. Due to imbalance in the number of UAV-view and satellite-view images, we perform image augmentation on satellite-view images during training. A small Vision Transformer (ViT-S) pre-trained on the ImageNet [16] is employed as the backbone for feature extraction. The ASA module and the classification module are trained from scratch. Our model is learned by an SGD optimizer with a

Table 1. Cross-view image retrieval performance (%) of different methods.

Method	Year	Backbone	UAV-to-Satellite		Satellite-to-UAV	
			Recall@1	AP	Recall@1	AP
Zheng et al. [7]	2020	ResNet-50	58.49	63.31	71.18	58.74
LCM [8]	2020	ResNet-50	66.65	70.82	79.89	65.38
LPN [5]	2021	ResNet-50	75.93	79.14	86.45	74.79
PCL [9]	2021	ResNet-50	79.47	83.63	87.69	78.51
RK-Net (USAM) [11]	2022	ResNet-50	77.60	80.55	86.59	75.96
SGM [12]	2022	Swin-T	82.14	84.72	88.16	81.81
FSRA [6]	2022	Vit-S	84.51	86.71	88.45	83.37
ASA (Ours)	–	Vit-S	85.12	87.21	89.30	84.17

Table 2. Cross-view image retrieval performance (%) with different strategies.

Strategy	UAV-to-Satellite		Satellite-to-UAV	
	Recall@1	AP	Recall@1	AP
Uniform hard partition strategy	83.98	86.27	88.59	83.91
k-means hard partition strategy	84.97	87.12	88.16	83.85
k-means soft partition strategy	85.12	87.21	89.30	84.17

momentum of 0.9 and weight decay of 0.0005. The mini-batch size is set to 8. The learning rate is initialized to 0.003 and 0.01 for ViT-S and the rest layers, respectively. The model is trained for a total of 120 epochs and the learning rate is decayed by 0.1 after executing 70 epochs and 110 epochs.

4.4 Experimental results

Comparison with existing methods. Table 1 presents our model’s performance for bidirectional cross-view retrieval between UAV-view and satellite-view images, compared to the previous methods [5–9, 11, 12]. LCM [8] resizes input images into 384×384 , and the image scale utilized in the other methods is 256×256 . Methods in [5, 7–9, 11] all use ResNet-50 [17] as backbone to extract CNN features. Among them, methods in [7, 8] learn global features, while LPN [5], PCL [9], and RK-Net [11] achieve part matching by using the square-ring partition strategy, which is not robust to scale variations. The experimental results demonstrate the inferior performance of these methods [5, 7–9, 11]. FSRA [6] and SGM [12] adopt transformers as backbone and cluster patches into semantic parts with hard partition strategies. Our method performs better than FSRA [6] and SGM [12] on both tasks, even though SGM [12] employs a stronger backbone. In comparison to FSRA [6], both methods extract features with ViT-S backbone and utilize $3\times$ sampling strategy to expand satellite-view images during training. The superior results achieved by our method demonstrate that the proposed ASA module reasonably aggregate patches into part-level representations, thus improving the performance of part matching.

Ablation study. In this section, we investigate the effect of several key factors. First, we explore the effectiveness of the proposed soft partition strategy by com-

Table 3. Effect of the number of parts on cross-view image retrieval performance (%).

Number of parts (K)	UAV-to-Satellite		Satellite-to-UAV	
	Recall@1	AP	Recall@1	AP
1	72.11	75.59	79.46	71.83
2	85.12	87.21	89.30	84.17
3	84.73	86.88	88.45	83.55
4	84.48	86.74	87.59	83.22

Table 4. Cross-view image retrieval performance (%) with different image sizes.

Image Size	UAV-to-Satellite		Satellite-to-UAV	
	Recall@1	AP	Recall@1	AP
224×224	82.28	84.83	86.31	81.93
256×256	85.12	87.21	89.30	84.17
384×384	86.88	88.74	89.44	85.95
512×512	88.67	90.29	89.44	87.14

paring it with two baselines in Table 2. The baseline “Uniform hard partition strategy” uniformly groups patches into K parts according to the 1-dimensional semantic representation obtained by Eq. 4. The baseline “k-means hard partition strategy” utilizes the k-means clustering results for part partition. Both baselines take the average of patches within each part to generate part-level representations. As shown in Table 2, the proposed “k-means soft partition strategy” is more effective in aggregating part-level features and achieves optimal results for UAV visual geo-localization.

Next, we analyze the impact of the number of parts K on the cross-view image retrieval performance. As shown in Table 3, the performance is poor if K is set to 1, since the learned part cannot express representative semantics of the image. Our model achieves the optimal generalization performance when K is set to 2. We believe that the learned two parts indicate typical semantics of foreground and background.

Finally, we discuss the effect of different image sizes. As shown in Table 4, high-resolution images generally yield better results since they retain more fine-grained details at the cost of more memory resources and inference time. The performance of our method does not degrade significantly when the image size is reduced from 512 to 256. Therefore, we recommend using the image size of 256 if hardware resources are limited.

5 Conclusion

In this paper, we have presented an adaptive semantic aggregation method to learn global-aware part-level features that can express typical semantics of scenes. Unlike the existing hard partition strategies, we have developed a soft partition strategy that searches for the most representative semantics as parts and evaluates the significance of patches to different parts. Our method adaptively aggregates features of all patches into part-level representations. Compared

to current works, the proposed method has achieved superior performance on the University-1652 dataset. Ablation studies also verified effectiveness of the proposed soft partition strategy and investigated several key factors of our methods.

References

1. Chivasa, W., Mutanga, O., Biradar, C.: Uav-based multispectral phenotyping for disease resistance to accelerate crop improvement under changing climate conditions. *Remote sensing* **12**(15), 2445 (2020)
2. Rizk, M., Slim, F., Charara, J.: Toward ai-assisted uav for human detection in search and rescue missions. In: DASA. pp. 781–786. IEEE (2021)
3. Ecke, S., Dempewolf, J., Frey, J., Schwaller, A., Endres, E., Klemmt, H.J., Tiede, D., Seifert, T.: Uav-based forest health monitoring: A systematic review. *Remote Sensing* **14**(13), 3205–3249 (2022)
4. Chiu, L.C., Chang, T.S., Chen, J.Y., Chang, N.Y.C.: Fast sift design for real-time visual feature extraction. *TIP* **22**(8), 3158–3167 (2013)
5. Wang, T., Zheng, Z., Yan, C., Zhang, J., Sun, Y., Zheng, B., Yang, Y.: Each part matters: Local patterns facilitate cross-view geo-localization. *TCSVT* **32**(2), 867–879 (2021)
6. Dai, M., Hu, J., Zhuang, J., Zheng, E.: A transformer-based feature segmentation and region alignment method for uav-view geo-localization. *TCSVT* **32**(7), 4376–4389 (2022)
7. Zheng, Z., Wei, Y., Yang, Y.: University-1652: A multi-view multi-source benchmark for drone-based geo-localization. In: ACM MM. pp. 1395–1403 (2020)
8. Ding, L., Zhou, J., Meng, L., Long, Z.: A practical cross-view image matching method between uav and satellite for uav-based geo-localization. *Remote Sensing* **13**(1), 47 (2020)
9. Tian, X., Shao, J., Ouyang, D., Shen, H.T.: Uav-satellite view synthesis for cross-view geo-localization. *TCSVT* **32**(7), 4804–4815 (2021)
10. Zhuang, J., Dai, M., Chen, X., Zheng, E.: A faster and more effective cross-view matching method of uav and satellite images for uav geolocalization. *Remote Sensing* **13**(19), 3979 (2021)
11. Lin, J., Zheng, Z., Zhong, Z., Luo, Z., Li, S., Yang, Y., Sebe, N.: Joint representation learning and keypoint detection for cross-view geo-localization. *TIP* **31**, 3780–3792 (2022)
12. Zhuang, J., Chen, X., Dai, M., Lan, W., Cai, Y., Zheng, E.: A semantic guidance and transformer-based matching method for uavs and satellite images for uav geo-localization. *IEEE Access* **10**, 34277–34287 (2022)
13. Bromley, J., Guyon, I., LeCun, Y., Säckinger, E., Shah, R.: Signature verification using a” siamese” time delay neural network. *Neurips* **6** (1993)
14. Koch, G., Zemel, R., Salakhutdinov, R., et al.: Siamese neural networks for one-shot image recognition. In: ICML deep learning workshop. vol. 2. Lille (2015)
15. Dosovitskiy, A., Beyer, L., Kolesnikov, A., Weissenborn, D., Zhai, X., Unterthiner, T., Dehghani, M., Minderer, M., Heigold, G., Gelly, S., et al.: An image is worth 16x16 words: Transformers for image recognition at scale. *arXiv preprint arXiv:2010.11929* (2020)
16. Deng, J., Dong, W., Socher, R., Li, L.J., Li, K., Fei-Fei, L.: Imagenet: A large-scale hierarchical image database. In: CVPR. pp. 248–255. IEEE (2009)
17. He, K., Zhang, X., Ren, S., Sun, J.: Deep residual learning for image recognition. In: CVPR. pp. 770–778 (2016)